Remote Sensing of Environment 114 (2010) 2457–2473

Contents lists available at ScienceDirect

Remote Sensing of Environment

journal homepage: www.elsevier.com/locate/rse

Mapping tropical dry forest height, foliage height profiles and disturbance type and age with a time series of cloud-cleared Landsat and ALI image mosaics to characterize avian habitat

E.H. Helmer [a,*], Thomas S. Ruzycki [b], Joseph M. Wunderle Jr. [a], Shannon Vogesser [b], Bonnie Ruefenacht [c], Charles Kwit [d,1], Thomas J. Brandeis [e], David N. Ewert [f]

[a] International Institute of Tropical Forestry, USDA Forest Service, Río Piedras, Puerto Rico 00926
[b] Center for Environmental Management of Military Lands, Colorado State University, Fort Collins, CO 80523, United States
[c] Remote Sensing Applications Center, USDA Forest Service, Salt Lake City, UT 84119, United States
[d] Department of Botany, Miami University, Oxford, OH 45056, United States
[e] Southern Research Station, USDA Forest Service, Knoxville, TN 37919, United States
[f] The Nature Conservancy, Lansing, MI 48906, United States

ARTICLE INFO

Article history:
Received 29 December 2009
Received in revised form 20 May 2010
Accepted 22 May 2010

Keywords:
Cloud-free image mosaics
Composite imagery
Merged imagery
Image fusion
Visualization
Change detection
Forest disturbance
Land-cover change
Normalized difference moisture index
NDSI
Normalized difference vegetation index
NDVI
Normalized difference structure index
NDSI
Normalized Difference Infrared Index
NDII
Avian habitat
Kirtland's Warbler

ABSTRACT

Remote sensing of forest vertical structure is possible with lidar data, but lidar is not widely available. Here we map tropical dry forest height (RMSE = 0.9 m, R^2 = 0.84, range 0.6–7 m), and we map foliage height profiles, with a time series of Landsat and Advanced Land Imager (ALI) imagery on the island of Eleuthera, The Bahamas, substituting time for vertical canopy space. We also simultaneously map forest disturbance type and age. We map these variables in the context of avian habitat studies, particularly for wintering habitat of an endangered Nearctic-Neotropical migrant bird, the Kirtland's Warbler (*Dendroica kirtlandii*). We also illustrate relationships between forest vertical structure, disturbance type and counts of forage species important to the Kirtland's Warbler. The ALI imagery and the Landsat time series are both critical to the result for forest height, which the strong relationship of forest height with disturbance type and age facilitates. Also unique to this study is that seven of the eight image time steps are *cloud-cleared images*: mosaics of the clear parts of several cloudy scenes. We created each cloud-cleared image, including a virtually seamless ALI image mosaic, with regression tree normalization. We also illustrate how viewing time series imagery as red–green–blue composites of tasseled cap wetness (*RGB wetness composites*) aids reference data collection for classifying tropical forest disturbance type and age. Our results strongly support current Landsat Program production of co-registered imagery, and they emphasize the value of seamless time series of cloud-cleared imagery.

Published by Elsevier Inc.

1. Introduction

Forest age, vertical structure, disturbance, and species composition are related forest attributes that affect avian habitat (Holmes et al., 1979; Johnston & Odum, 1956; Karr, 1968; Leck, 1979; MacArthur, 1958; Rappole & Morton, 1985; Terborgh, 1977; Thiollay, 1999). Studies often characterize avian habitat by mapping these variables with remote sensing (Bergen et al., 2007; Goetz et al., 2007; Gottschalk et al., 2005). Here we describe a study to map these variables in a persistently cloudy tropical region with remote sensing data that are widely and freely available.

Algorithms can now automatically map forest disturbance that is stand replacing, or forest age, with time series of mostly cloud-free Landsat images (Helmer et al., 2009; Huang et al., 2009; Kennedy et al., 2007; Masek et al., 2008). One possibility to minimize cloud contamination, especially in more cloudy regions, is to mosaic or composite multiple images which can now be done without concern for image costs, as long as data come from the U.S. Geological Survey (USGS) or the Brazilian Institute for Space Research. Here we refer to

* Corresponding author.
E-mail address: ehelmer@fs.fed.us (E.H. Helmer).
[1] Current address: Department of Plant Sciences, University of Tennessee, Knoxville, TN 37996, United States.

0034-4257/$ – see front matter. Published by Elsevier Inc.
doi:10.1016/j.rse.2010.05.021

such images as *cloud-cleared images*. Also, it is now feasible to create long time series of cloud-cleared images, perhaps with intervals of ≤5 years in cloudy tropical regions if other receiving stations make their Landsat archives freely available. Yet whether long time series of cloud-cleared Landsat images will permit us to map simultaneously tropical forest change between many time intervals is untested.

In this study, we create a time series of cloud-cleared images and test if we can use it to map forest attributes important to avian habitat, including forest vertical structure and disturbance type and age. Landsat Thematic Mapper (TM), Enhanced Thematic Mapper (ETM+) and Advanced Land Imager (ALI) images compose the cloud-cleared images. Only one nearly clear image exists for the study area. Recent studies suggest that where clear scenes are rare, cloud-cleared images and cloud-cleared image time series are as valuable for monitoring forests as clear images or image time series. Helmer and Ruefenacht (2005) detect land-cover change to developed lands with simple maximum likelihood classification of two time steps of cloud-cleared images. For each image time step, regression tree models predict pixel values of a reference, or *base* scene, from the clear parts of *secondary* scenes that can fill areas obscured by clouds in the base scene. Hansen et al. (2008) detect forest clearing with two time steps of cloud-cleared imagery by classifying each time step into forest vs. nonforest. Accurate land-cover and forest type mapping is also possible with cloud-cleared imagery. Recent work simultaneously maps land cover and many different forest habitats in persistently cloudy, complex tropical regions with decision tree classification of cloud-cleared Landsat imagery and ancillary data, like digital elevation model-(DEM) derived variables (Helmer et al., 2008b; Helmer & Ruefenacht, 2007; Kennaway & Helmer, 2007; Kennaway et al., 2008).

Methods for remote sensing of forest height use lidar (Lefsky et al., 2002), radar imagery (Kellndorfer et al., 2004; Papathanassiou & Cloude, 2001), multi-angle and seasonal optical imagery with coarse spatial resolution (Chopping et al., 2009), aerial photos (Véga & St-Onge, 2008), optical imagery with fine spatial resolution (Wolter et al., 2009), or sometimes single-date optical imagery with medium spatial resolution (Kalacska et al., 2007). Of these data, only lidar directly measures the vertical distribution of forest canopies. Unfortunately, spatially contiguous lidar data are not globally available and were not available for this study. Multispectral optical satellite imagery is globally available, but its sensitivity to forest height is limited. What scientists have not tested is whether time, in the form of multiyear image time series, can substitute for vertical canopy space for mapping forest vertical structure with globally available, multispectral optical imagery. After stand-clearing disturbances, young forest spectral responses change as they grow taller and denser. Consequently, the pattern of spectral responses over time should be related to forest height.

Our application is a project to map forest attributes important to habitat of the Kirtland's Warbler (*Dendroica kirtlandii*), the endemic Bahama Yellowthroat (*Geothlypis rostrata*) and other migrant and resident bird species of broadleaved dry tropical forests of The Bahamas. The Kirtland's Warbler is an endangered Nearctic-Neotropical migrant that is the target of extensive conservation efforts on its limited breeding grounds in Michigan and Wisconsin, U.S.A. and in Ontario, Canada. It winters exclusively in the Bahamian archipelago. Only recently have data been available on wintering habitat use by this species; these data suggest that the Kirtland's Warbler frequents disturbed habitats (Wunderle et al., 2007, 2010).

Our main objectives are to test if we can use a time series of cloud-cleared multispectral images to: 1) simultaneously map forest disturbance type, age and land cover; 2) map forest vertical structure from field-measured foliage height profiles, substituting the image time series for vertical canopy space; and 3) illustrate relationships between forest disturbance type, vertical structure and profile counts of woody species that characterize Kirtland's Warbler habitat. Secondary objectives include comparing mapping models based on single-date imagery with those based on an image time series and qualitatively evaluating cloud-cleared ALI imagery made with the regression tree normalization method of Helmer and Ruefenacht (2005). Imagery from ALI has the same, 12-bit multispectral bands as the Operational Land Imager (OLI) that will be aboard the next Landsat mission. Finally, the map of forest disturbance type and age allows us to estimate for the first time disturbance rates for broadleaved forests that the Kirtland's Warbler occupies in winter.

2. Methods

2.1. Study overview

First, we create an eight-step image time series from 24 Landsat and Advance Land Imager (ALI) scenes. Seven of the eight time steps

Table 1
We created an eight-step image time series from the 24 scenes listed here, along with their cloud cover over land, by producing cloud-cleared image mosaics. The study area encompassed a portion of path/row 012/043 in World Reference System 2. Each mosaic included a reference, or *base* scene. The clear parts of scenes from other dates, or *secondary* scenes, then filled the cloudy parts of the base scene after undergoing normalization to the base scene with the regression tree method of Helmer and Ruefenacht (2005). Secondary scenes are listed in the order that they filled cloudy areas in the base scene (i.e., top to bottom). Scene types: L4 = Landsat 4 Thematic Mapper (TM); L5 = Landsat 5 TM; L7 = Landsat 7 Enhanced TM; and ALI = Advanced Land Imager.

Base year of time step	Base scene date (month/day/yr) and image type of time step	Base scene cloud cover over study area (%)	Dates and types of secondary scenes that fill clouds in corresponding base scenes (month/day/yr)	Secondary scene cloud cover over study area[a] (%)	Cloud cover in final mosaic (%)
1984	06/03/1984–L5	0.1	–	–	0.1
1988	12/15/1988–L4	42	04/03/1988–L4	16	3.6
1993	11/19/1993–L5	31	12/05/1993–L5	29	0.1
			01/22/1994–L5	35	
			02/23/1994–L5	39	
			03/11/1994–L5	45	
			12/08/1994–L5	35	
1996	12/29/1996–L5	25	12/27/1995–L5	15	0.2
			01/28/1996–L5	17	
2000	03/11/2000–L5	20	02/08/2000–L5	17	0.0
			11/28/1999–L7	22	
2001	03/06/2001–L7	15	02/02/2001–L7	23	0.7
			11/17/2001–L7	45	
2002	11/04/2002–L7	1.2	01/23/2003–L7	21	0.0
2005	04/11/2005–ALI	23[a]	05/04/2005–ALI	42[a]	12[a]
			05/29/2005–ALI	38	
			01/15/2006–ALI	56	

[a] Includes land in northern Central Eleuthera with neither clear nor cloudy image data available.

Table 2
The mapping models tested in this study, and their associated input bands, are listed here. The input bands for each classification or regression tree mapping model are represented by the image type and mosaic date. Input bands for Thematic Mapper (TM) and Enhanced Thematic Mapper included bands 1–5 and 7 and the Tasseled Cap Brightness, Greenness and Wetness indices. Advanced Land Imagery (ALI) bands included all 30-m optical bands and two band indices: NDVI and NDSI (see text).

Model number	Mapping models tested and associated input variables
See5 decision tree classification models of land cover and forest disturbance type and age	
(1)	Class = f {TM_{1984}, TM_{1988}, TM_{1993}, TM_{1996}, TM_{2000}, ETM_{2001}, ETM_{2002}, ALI_{2005}}
(2)	Class = f {ETM_{2002}}
(3)	Class = f {TM_{1984}, TM_{1988}, TM_{1993}, TM_{1996}, TM_{2000}, ETM_{2001}, ETM_{2002}}
Cubist regression tree models of mean canopy height (m)	
(4)	Height = f {TM_{1984}, TM_{1988}, TM_{1993}, TM_{1996}, TM_{2000}, ETM_{2001}, ETM_{2002}, ALI_{2005}}
(5)	Height = f {ALI_{2005}}
(6)	Height = f {ETM_{2002}}
(7)	Height = f {TM_{1984}, TM_{1988}, TM_{1993}, TM_{1996}, TM_{2000}, ETM_{2001}, ETM_{2002}}
Cubist regression tree models of foliage height profiles (mapped as percent foliage cover over six height intervals) and height variance	
(8)	Height variance = f {TM_{1984}, TM_{1988}, TM_{1993}, TM_{1996}, TM_{2000}, ETM_{2001}, ETM_{2002}, ALI_{2005}, height, disturbance type, disturbance/forest age}
(9) to (14)	[a]Percent cover$_i$ = f {TM_{1984}, TM_{1988}, TM_{1993}, TM_{1996}, TM_{2000}, ETM_{2001}, ETM_{2002}, ALI_{2005}, height, disturbance type, disturbance/forest age}

[a] i = height interval, including: 0–1 m, 2–3 m, 3–4 m, 4–6 m or >6 m.

are cloud-cleared image mosaics (Table 1). Second, we simultaneously map land cover and forest disturbance type and age with a single decision tree classification of the stack of optical bands from all eight of the image time steps (Table 2, Model 1). We also explore if the mosaic time series was important to mapping forest disturbance type and age as compared to using imagery from only a single mosaic time step (comparing Models 2 and 3 in Table 2). Third, we measure foliage height profiles at 48 field forest plots representing a range of forest disturbance types and ages, also counting occurrences of five woody species that may affect Kirtland's Warbler habitat. Fourth, we map variables from the foliage height profiles, like mean canopy height (Model 4), height variance (Model 8), and percent cover over various height intervals (Models 9–14), with regression tree classification of the stack of image bands from the time series. Here also we test whether the image time series is important, in this case to mapping forest height (comparing Models 4–7). Fifth, we use principal components analysis (PCA) to illustrate the relationships between forest disturbance type, vertical structure and counts of the five woody species. Finally, we estimate forest disturbance rates.

2.2. Study area

The geology and topography of Eleuthera (25° N, 76° W) are typical of The Bahamas, a country consisting of a chain of oceanic, low elevation, limestone islands that lie off the southeastern coast of the U.S. state of Florida and extend to northeastern Cuba. Eleuthera has a subtropical dry climate with a mean annual temperature of about 24 °C and annual precipitation ranging from 1100 to 1300 mm year^{-1}. Vegetation is typical of dry, broadleaved semi-evergreen secondary forest on limestone substrate of the West Indies. The diverse flora includes deciduous and hard-leaved evergreen tree and shrub species. A few common canopy species in these diverse forests are *Bursera simaruba*, *Coccoloba diversifolia*, *Metopium toxiferum*, *Guapira obtusata*, *Pithecellobium keyense*, *Lysiloma latisiliquum*, *Eugenia axilaris*, *Piscidia piscipula*, *Bourreria ovata*, *Bumelia salicifolia*, *Amyris elemifera*, *Reynosia septentrionalis*, *Exothera paniculata*, and *Exothema caribeaum*.

Increasing forest cover after the year 1950 is typical of Caribbean islands (Helmer et al., 2008a,b), including Eleuthera. Settled in 1648, pineapple cultivation and pasture were extensive there until the mid-1900s, when economic and political forces led to a decline in agriculture and an increase in forest cover. In recent decades, forest clearing for agriculture consists of bulldozing or cutting for small fields followed by slash burning. Farmers cultivate fields for a short time while woody species resprout, and while forbs, shrubs and trees colonize the fields, before eventual field abandonment. Slash burning leads to forest disturbance by escaped fire. Forest clearing also occurs for goat grazing and for residential development that may or may not follow. Goat grazing and browsing do not prevent re-establishment of a dense woody vegetation canopy. For these forest disturbances, time since last disturbance yields a good estimate of recovering forest age in the study area. Forest clearing for citrus plantations is an exception, because farmers clear non-crop vegetation while the plantations are active. Hurricanes have also disturbed forests on Eleuthera in the past 40 years. Though we observed little direct evidence of hurricane disturbance in the Landsat images, some indirect evidence of hurricane disturbance may be present in the Landsat record (see Section 3.6).

2.3. Creating a cloud-free Landsat and ALI image time series where clear scenes are rare

Few methods normalize nonlinear differences in vegetation phenology between the image dates that compose cloud-cleared imagery. However, normalizing imagery with respect to phenology aids visual image interpretation when collecting reference data (Helmer & Ruefenacht, 2007), which is important to this study. Normalizing the phenology of the image data that composes image composites or mosaics should also yield more effective models of forest attributes that are based on limited field data. One method is the regression tree normalization approach that we use here (see below), which Helmer and Ruefenacht (2005) describe in detail. Subsequent studies use the image mosaics resulting from the method to map land cover and detailed forest types in complex tropical landscapes (Helmer et al., 2008b; Kennaway & Helmer, 2007; Kennaway et al., 2008). Helmer and Ruefenacht (2007) show that the method more closely matches vegetation phenology between scenes from different dates than do linear methods for image normalization, including linear regression, linear histogram matching, or atmospheric correction by dark object subtraction. A second approach to fusing imagery adjusts the imagery via the relationships between co-located pixels from two Moderate Resolution Imaging Spectroradiometer (MODIS) images (Gao et al., 2006; Roy et al., 2008). The two MODIS images have dates close to those of the base Landsat scene and the Landsat scene that will fill gaps in the base scene. This latter approach, though, is not applicable for time steps dated over the 28 years from 1972 to 1999, before MODIS data became available. Localized histogram matching methods, developed to fill scan gaps in ETM+ images dated after May 2003, and co-kriging approaches (Zhang et al., 2009), assume that the pixels surrounding an image gap have brightness value distributions that are similar to those within the gap. Large cloud gaps often violate this assumption. Interpolating pixel values between image time steps dated before and after a cloudy pixel avoids the need for cloud-cleared imagery (e.g., Huang et al., 2009). This approach might miss forest disturbance if regrowth is fast enough.

We created an eight-step time series of Landsat and ALI imagery consisting of seven cloud-cleared mosaics and an eighth clear image (Table 1). We produced each cloud-cleared image mosaic with the regression tree normalization method of Helmer and Ruefenacht (2005). Each time step has one base scene. The base scenes were dated from 1984 to 2005 and spaced at intervals of ≤5 years. The regression tree method predicts pixel values for cloudy areas in each base scene from pixels that are clear in the secondary scenes for each time step with a Cubist (www.rulequest.com) regression tree model for each band. The basis for each model is the set of co-located, mutually clear pixels from each base- and secondary-scene pair. The regression tree models for Landsat Thematic Mapper (TM) or Enhanced Thematic Mapper (ETM+) scenes, for example, have the following general form:

$$y_{basei} = f(x_{sec1}, x_{sec2}, x_{sec3}, x_{sec4}, x_{sec5}, x_{sec7}) \quad (1)$$

In Eq. (1), y_{basei} is the digital number (DN) of a pixel in the base scene for the *i*th band to be predicted, x_{sec1} is the DN of the TM or ETM+ band 1 of the corresponding pixel in the secondary scene, x_{sec2} is the DN for band 2 of the secondary scene, and so on. Here one to five secondary scenes dated within 13 months of the base scene fill cloudy areas in the base scene. The base scenes have less than about 30% cloud cover and are dated from November to March, corresponding to the early to mid-dry season before peak leaf loss of deciduous species.

We masked clouds and cloud shadows from all scenes with image-specific thresholds in various bands followed by manual editing. We identified clouds with maximum thresholds in a thermal band in TM imagery and minimum thresholds in the blue MS2 band for ALI images. Manual editing added warm or thin clouds to the resulting cloud masks and removed patches misclassified as cloud. We identified cloud shadows with maximum thresholds in a shortwave infrared (SWIR) band, including TM/ETM+ band 5 or ALI band MS5. Manual editing removed shallow water and some wetlands from the resulting cloud shadow mask. We then co-registered all scenes to the reference scene for the year 2000 mosaic with ERDAS Imagine Autosync (ERDAS, 2008), using the red band for finding tie points and with nearest neighbor resampling. Root mean square errors (RMSE) for the co-registrations were <0.5 pixels. We then normalized the secondary scenes to the base scene for each mosaic time step with a regression tree model. The Landsat TM and ETM+ scenes had a spatial resolution of 28.5 m, and we resampled the 30-m ALI image mosaic to 28.5 m. The Landsat and ALI imagery came from the USGS.

2.4. Mapping land cover, forest age and forest disturbance type with an image time series

We simultaneously mapped land cover and forest disturbance type and age by classifying a 74-band stack from the cloud-cleared image time series (Model 1, Table 2). We calculated forest disturbance rates as the number of ha disturbed during an interval divided by the interval length. Section 3.2 in the results has a complete list of the classes mapped. Reference data for training and accuracy assessment came from: 1) field work in May 2005, August 2006, November 2006 and March 2007; 2) Quickbird imagery for South Eleuthera dated November 2004 to May 2005; 3) Quickbird imagery viewable on Google Earth and dated from 2004 to 2005 (see Helmer et al., 2009 on using Google Earth for validation and training data); and 4) viewing the image sequence of cloud-cleared images as *RGB wetness composites*, which we describe in the next section.

These training data included 20 to 50 multi-pixel patches distributed throughout each class. Forest classes with no disturbance during the image sequence included four wetland and one upland forest class. Forest classes disturbed during the image sequence included one burned wetland class and a separate class for each of four disturbance types and up to nine disturbance/forest ages. Disturbance types included: 1) bulldozing or larger-scale clearing for agriculture, pasture, or intended (but not occurring) residential development, followed by forest regrowth; 2) clearing and burning without bulldozing, also followed by regrowth; 3) burning from escaped fire, and 4) clearing for goat pasture followed by regrowth with continued goat grazing. Most agriculture patches smaller than 1 ha are patches of mixed vegetable crops called *conucos. Conuco* is a Taino Indian term for a small plot of cultivated land. Because clearing for conucos may or may not include bulldozing, they fall into both of the first two disturbance types. The nine age classes included young forest recovering from recent disturbance in 1984, forest recovering on land that was not forest in 1984 (see next section on distinguishing these two classes), and forest recovering from disturbance during each of the seven intervals between the mosaics. Young forest classes could have less than 60% woody vegetation cover. Nonforest classes included urban or built-up land; land converted to urban or built-up land between 1984 and 2005; golf course or other grass; bare land; water; active cattle pasture with less than 25% woody vegetation; and active cattle pasture with 25 to 60% woody vegetation. We manually delineated the few active or recently active citrus plantations. Two large areas subject to two escaped fires were kept as separate classes. Other areas of repeated disturbance were too few and too small to keep as separate classes.

For the classification, we used the decision tree classification software See5 (www.rulequest.com). See5 uses training data to form a decision tree and associated rulesets that classify data. The nodes in the tree are based on whichever predictor variable splits the training data in a way that maximizes information gain (Kullback, 1959); the subsets that result from nodes each contain more or less of a given class or classes. We applied the decision tree model with an ERDAS Imagine module from Ruefenacht et al. (2008), which applies a See5 classification tree to a stack of raster data in ERDAS Imagine format. The 74 layers came from the nine multispectral bands plus two indices from the ALI image mosaic plus the six optical bands and the tasseled cap (TC) brightness, greenness and wetness indices (Crist & Cicone, 1984; Crist et al., 1986; Huang et al., 2002) from each of the TM or ETM+ mosaics. The TC equation applied to a given mosaic was the equation appropriate for its base image. We calculated TC indices from DNs for mosaics with TM base scenes and from top-of-atmosphere reflectance for mosaics with base scenes from ETM+. The two ALI indices were a normalized difference vegetation index (NDVI), calculated from the near infrared (NIR) MS4 band (0.775–0.805 nm) and the red band (MS3, 0.633–0.69 nm). The second index relates to leaf water content, water levels in saturated or inundated soils, and forest structure. It is referred to as the *normalized difference infrared index* in Hardisky et al. (1983) and the *normalized difference moisture index* in Wilson and Sader (2002). Because this index relates strongly to forest height in this study, we refer to it here as the *normalized difference structure index* (NDSI), after the *structural index* (Landsat TM band 4:5 ratio) of Fiorella and Ripple (1993a,b). For ALI, the NDSI derives from the NIR MS4 and the SWIR MS5 bands, as follows:

$$\text{NDSI} = (\text{MS4} - \text{MS5}) / (\text{MS4} + \text{MS5}) \quad (2)$$

We produced two accuracy estimates. First, we estimated pixel-level accuracy as the overall accuracy of the classification model that resulted if we withheld a randomly selected 30% of the training data. Second, a stratified random sample of about 30 points per class provided data for an independent error assessment. Neither accuracy estimate accounted for inclusion probability or for any spatial autocorrelation that might exist among reference data. We designed the stratified sample to represent more closely errors at the level of patches rather than pixels. The design stemmed from earlier work (Wunderle et al., 2010) that applied a 3×3 majority filter to the final map to avoid assigning a nonforest class to Kirtland's Warbler capture sites that fell on pixels that were a mixture of forest and nonforest.

Consequently, the stratified sample was limited to points in a class that held a majority within the surrounding 3×3-pixel window (7310 m^2). With this sample design, the error estimates from the stratified sample apply only to pixels that are part of a majority within the 3×3-pixel window surrounding them.

When collecting the points for the stratified random sample, a search of 5×10^5 randomly generated points often found fewer than 30 points for classes with small total areas. In those cases, we kept the points that the search located but did not search further, to avoid oversampling those classes (R. Czaplewski, personal communication). This approach yielded few points for some ages of non-bulldozed, small-scale agriculture and some ages of goat-grazed forest. As a result, we combined the validation points for forest recovering from bulldozing for agriculture with those that recovering from clearing only. As for goat-grazed forest patches, they were concentrated in a few known areas, so we also qualitatively evaluated their accuracy at the patch level. We also doubled the number of points for forest undisturbed during the image sequence, the most extensive class. For the error assessment data from the stratified random sample, we calculated overall, producer's and user's accuracy, as well as the Kappa coefficient of agreement (Cohen, 1960) with the formula for a stratified random sample in Czaplewski (2003).

In addition to the above two accuracy assessments of the map of land cover and forest disturbance type and age, we also compared the results of using different band combinations for such mapping. We compared a model based on the bands from the mosaics spanning 1984 to 2002 with one based only on the mosaic from 2002 (comparing Models 2 and 3, Table 2). We based this comparison on a randomly withheld 30% of the training data. For this comparison, we excluded the ALI imagery from 2005 because no ALI data were available for the northernmost part of Central Eleuthera. We expected the mapping model based on the mosaic time series to be more accurate than the model based on a single image mosaic.

2.5. Identifying forest disturbance type and age with RGB wetness composites

To identify forest disturbance type and age for reference data, we viewed the imagery as red–green–blue (RGB) color composites of TC wetness (Jin & Sader, 2005), which we refer to here as *RGB wetness composites*. Like RGB–NDVI composites (Sader & Winne, 1992), RGB composites display an index, in this case TC wetness, from three sequential images in RGB color space. Scaling the display brightness in each band to range over that of forest (the mean plus or minus two standard deviations, including secondary forest), or simply applying a two-standard-deviation stretch to forest-dominated imagery, help to make the method fairly objective and repeatable. This scaling causes pixels with TC wetness values smaller than most forest to display brightness values close to zero. The relationships between forest disturbance and display color are identical in RGB wetness composites in Amazonia (Helmer et al., 2009), Maine (Jin & Sader, 2005) and Eleuthera (this study). Disturbance between dates one and two of a composite, without regrowth by date three, appears red. Disturbance with regrowth by date three appears magenta, and so on (Table 3, Fig. 1). Where woody species quickly colonize previously cleared land, including all but the driest tropical forest landscapes, pixels attain values of TC wetness or related indices that are visible as regrowth within a year or two.

Simultaneously viewing all three-band sequential combinations of TC wetness over a densely-spaced, long time series: 1) distinguishes forest from pasture and herbaceous or open woody agriculture, and 2) reveals forest age as the interval when forest regrowth begins that lasts through the image sequence (Helmer et al., 2009), which in Eleuthera is usually also the interval of last disturbance. Nonforest land, or land that changes to a nonforest use after forest clearing, has TC wetness that either remains small or does not increase over the long term, consistently appearing dark in all composites: black, red, green or dark blue (dark blue in the last composite of a sequence of composites may also indicate forest regrowth).

As for forest age, we calculated it as the time difference from March 2007, when we measured foliage height profiles, and the midpoint of the interval of the last disturbance, using the date of the base scene for each mosaic. When viewing the sequence of composites, the cyan of initial forest recovery first pales to lighter cyan or dark grey and then brightens toward the lighter grey of mature forest. This pattern allowed us to distinguish two ages of disturbed forest from the earliest image time step. Lands that were active agriculture or pasture in 1984 and regrew after 1984 are dark cyan in RGB wetness composites (e.g., patch 2 in Fig. 1c). Relative to forest, their TC wetness is dark in 1984 but brightens in 1988 and 1993. In contrast, young forest already recovering from disturbance before 1984 is pale cyan or dark grey, because its TC wetness is already within the range of forest in 1984 (e.g., patch 4 in Fig. 1c).

We assigned the oldest forest an age of 37 years by learning, from observing the image time series, how long disturbances remain discernable in the imagery. In the series, forest clearing with bulldozing becomes indiscernible from old forest by about 14 years after disturbance. Forest burned from escaped fire can become indiscernible within about 8 years. We consequently assumed that the oldest forest, which is forest with no sign of disturbance through the image sequence, was 8 to 14 years old in 1984, making it 31 to 37 years old or older in 2007.

Forest disturbance in a secondary scene that fills cloud gaps in a reference scene is assigned the age of the reference scene for a

Table 3
Interpretation of additive colors in three-date RGB–Wetness image composites (adapted from Sader & Winne, 1992; Wilson & Sader, 2002). Each RGB composite displays an index, in this case Tasseled Cap (TC) wetness or the NDSI, from three sequential images in RGB color space. To produce these colors, scale the display brightness in each band to range over that of forest, or apply a two-standard-deviation stretch to forest-dominated imagery.

Additive display color	TC wetness relative to forest in date 1 (red)	TC wetness relative to forest in date 2 (green)	TC wetness relative to forest in date 3 (blue)	Interpretation
Black	Low	Low	Low	Nonforest or open forest/savanna with low biomass and a senescent understory
Red	High	Low	Low	Nonforest or forest clearing from dates 1 to 2 without regrowth by date 3
Green	Low	High	Low	Nonforest or forest clearing before date 1, followed by regrowth and then clearing from dates 2 to 3
Blue	Low	Low	High	Nonforest or forest regrowth beginning between dates 2 and 3
Yellow	High	High	Low	Forest clearing from dates 2 to 3
Magenta	High	Low	High	Forest clearing from dates 1 to 2 with regrowth from dates 2 to 3
Pale magenta	High	Medium	High	Partial forest disturbance from dates 1 to 2 with regrowth from dates 2 to 3
Cyan	Low	High	High	Forest regrowth beginning between dates 1 and 2 and continuing through date 3
Pale cyan/dark grey	Medium	Medium to high	Medium to high	Young or partially disturbed forest in date 1 that continued to grow through dates 2 and 3
Grey/white	High	High	High	Grey: broadleaved forest (leaf-on) White: water, inundated forest, or evergreen needleleaf forest

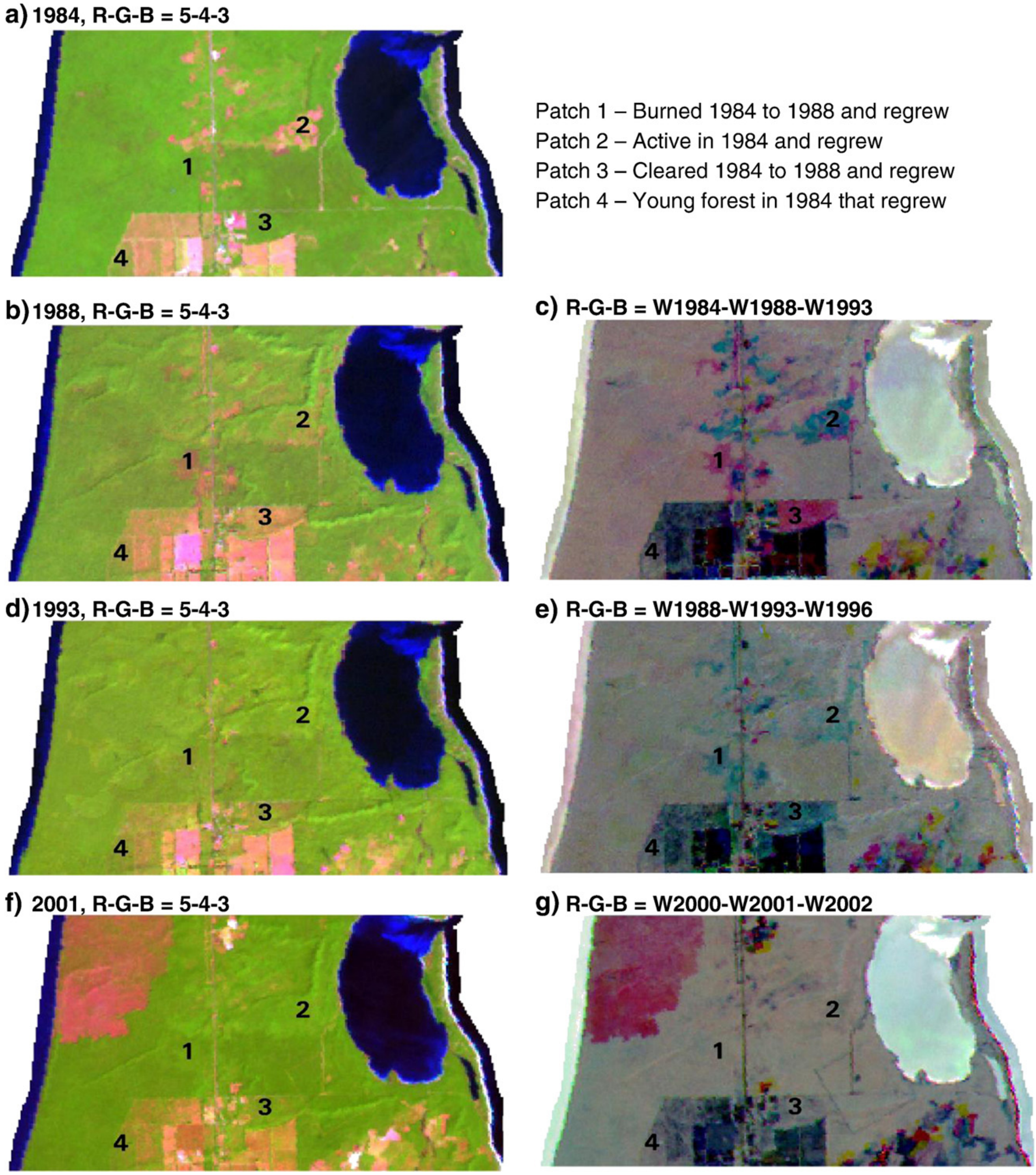

Fig. 1. *RGB wetness composites* (figures c, e and g) display three sequential dates of the Tasseled Cap Wetness index (W) in the red (R), green (G) and blue (B) display bands (e.g., R–G–B = W1984–W1988–W1993 displays W from 1984, 1988 and 1993 in R, G, B color space, respectively). Disturbance between composite dates one and two appears magenta; disturbance between composite dates two and three appears yellow; initial regrowth is cyan (if regrowth began between dates 1 and 2) to pale cyan. Also shown are TM bands 5, 4 and 3 in RGB for subsets of the image mosaics for the earliest date (1984) and for the middle date of each composite (1988, 1993 and 2001). Annotations 1 through 4 are described in the upper right corner of the figure. For interpretation of additional colors in this figure, the reader is referred to Table 3.

given mosaic. This age assignment is less precise than if clear data from a single image date were available for the entire study area for each time step in the series. For example, forest disturbance in a secondary scene that is dated some months after the base scene for a given mosaic is assigned an age that is older than the actual disturbance. Minimizing the time differences between the base scene and secondary scenes for each mosaic minimizes this error source.

To confirm disturbance types before 1996, we viewed single image dates. For later time steps, we determined disturbance type from the Quickbird imagery or field visits. Patches recently burned by escaped fire are clearly distinguishable from agricultural clearing. Their shape is irregular and their spectral signatures are darker than recently bulldozed land in all bands. Recently bulldozed patches are as bright as barren land. Agriculture patches that were cleared and burned but not obviously bulldozed are small and regularly shaped but as dark as escaped fire in visible bands. Field visits allowed us to identify goat-grazed patches.

In the RGB composites, we substituted the NDSI from ALI for TC wetness. Both indices increase directly with NIR reflectance and indirectly with SWIR reflectance. Indices that contrast NIR and SWIR reflectance are sensitive to forest stand development in various forest types. The NDSI and TC wetness tend to increase with stand age through mid-forest succession under leaf-on conditions, though in some forests TC wetness peaks in mid-forest succession or when forest canopies close, and then decreases slightly in late succession (Fiorella & Ripple, 1993a,b; Helmer et al., 2000; Wilson & Sader, 2002).

In humid tropical landscapes, where active or semi-active woody agriculture may form a dense woody canopy, distinguishing forest from active or semi-active woody agriculture can be difficult, even with an image time series and RGB wetness composites (Helmer et al., 2009). Finally, agriculture that forms a tall dense herbaceous canopy at peak development, like sugar cane, might also be indistinct from young forest if all images in a sequence occur at peak crop development.

2.6. Mapping tropical dry forest height and foliage height profiles with time series imagery

To calibrate mapping models for forest vertical structure and explore the relationships between forest vertical structure and disturbance type, age and counts of selected woody species, we measured foliage height profiles at 48 plots in March 2007 (Fig. 2). From the data for each foliage height profile plot, we calculated the following variables (see details below): mean height, height variance, percent foliage cover for each height interval, and total counts of five woody species potentially affecting Kirtland's Warbler habitat.

Although the number of profile plots was somewhat small, we used a stratified random sample design to ensure that the plots represented the range of the most common forest disturbance histories in South Eleuthera. The patch level, stratified random sample design for the foliage height profile plots came from a contiguity analysis of the map of forest disturbance type and age. A contiguity analysis assigns the pixels in each contiguous region of the same class an individual value. We grouped patches of forest younger than 37 years into six groups, depending on whether they were disturbed before or after the year 2000 and whether the disturbance was clearing for agriculture of any kind, escaped fire, or clearing followed by continued goat grazing. We then randomly sampled patches until we had sampled at least three to five patches per group, excluding patches that were misclassified or inaccessible. When we excluded such patches, we visited the next patch in a random sorting of the patches in each group. Inaccessible plots included those for which access was denied by landowners and those that were either too distant from our field base, given available time for fieldwork, or more than two km from a road. Bias in the resulting sample is toward patches that are more accessible. In stratifying the sample by age, however, the sample design mitigates this bias, because tropical forest age is strongly related to accessibility (Helmer, 2000; Helmer et al., 2008a). To sample forests at least 37 years old, which form the matrix of the forest landscape in South Eleuthera, we located plots in a random direction and distance (<200 m but >25 m) to the north of Madera Rd., which borders extensive old forest. For all of the younger forest plots, plot centers were located within the patch and at least 45 m from the patch edge.

Fig. 2. Foliage height profiles were measured for 48 plots that represented the range of the most common forest disturbance types and ages in South Eleuthera, The Bahamas.

Foliage height profiles were measured with the method of Schemske and Browkaw (1981) as modified by Wunderle and Waide (1993). Each plot consists of two perpendicular transects centered at the plot center. Along each transect are 20 points spaced at 1, 2, 3, 4 and 5 m from the plot center. Whether or not foliage touches a vertical pole is recorded in height increments up the pole. The height increments are at 0.5-m increments from 0 to 3 m above the ground, and in subsequent height increments of 3–4, 4–6, 6–8, 8–10, and >10 m. This plot size is smaller than the multispectral Landsat or ALI pixels. However, plot locations were in patches of uniform disturbance type and age, minimizing the potential impacts of this spatial mismatch. Mean canopy height is the mean over the 20 points of the midpoints of the highest increment in which foliage touches the pole. Height variance is the variance of the mean height. Percent cover for each height increment is the percent of the 20 points in which any foliage touches the pole. Studies of Kirtland's Warbler foraging suggest that the fruit of four woody species are important winter forage for the species. Consequently, we counted the number of times that the four forage species touched the pole in any of the 20 points for each plot. The four species were *Chiococca alba*, *Erithalis fruticosa*, *Lantana involucrata*, and *L. bahamensis*. We also counted hits of the non-native *Leucaena leucocephala*, because it may compete with the forage species in early succession.

We mapped variables from the foliage height profiles with Cubist regression tree models. Predictor variables for forest height included only the 74 optical layers used to map forest disturbance type and age. We then added mapped forest height, and mapped forest disturbance type and age, to the set of predictor variables for mapping foliage cover of six height intervals and height variance. A 10-fold cross-validation provided data for evaluating these regression tree mapping models. Cross-validation may slightly overestimate the correlation between actual and predicted values in the mapping models, but the number of forest plots was too small to divide the reference data into separate training and testing subsets.

2.7. Illustrating the relationships between forest vertical structure and Kirtland's Warbler forage species

To illustrate the relationships between forest vertical structure, disturbance type, and counts of the woody species tallied in the profile plots, we applied principal components analysis (PCA) to the height profile data. Because the species counts inherently depend partly on foliage cover, multiple regression analysis was inappropriate for this purpose. Principal components analysis transforms multivariate data into independent axes, condensing many related, often redundant variables into a few axes that explain much of the variability in a dataset (Legendre & Legendre, 1998). Plotting the principal component scores for observations then reveals the major gradients in a dataset. The transformation coefficients for each variable, which are the factor loadings, are correlation coefficients between the original variables and the gradients, revealing their relationship to each other. With PCA, variables can have different measurement units. In this case, the units include percent foliage cover and species counts. The main assumption of PCA is that the variables relate linearly to one another. Consequently, PCA is suitable for analyzing species abundances over gradients that are short enough for the abundances to increase or decrease monotonically along their length (Legendre & Legendre, 1998). In this case, excluding foliage cover in intervals above 4 m shortens the environmental gradient enough to allow the data to meet this requirement. We also excluded *E. fruticosa* because the data had few observations of this species.

The axes of the resulting PCA are gradients that relate forest vertical structure to abundances of species potentially important to Kirtland's Warbler habitat. Earlier work applies PCA to a dataset that combines foliage height profiles from Kirtland's Warbler capture sites with the randomized plots collected for this study (Wunderle et al., 2010). The PCA here differs from that work by excluding the capture site data to obtain a more balanced dataset. The capture sites bias toward places the bird inhabits and span several years. In addition, this PCA uses the height intervals collapsed to those that we map here, and it includes counts of the forage species and *L. leucocephala*.

3. Results and discussion

3.1. Cloud-free ALI image mosaic and regression tree normalization

The cloud-cleared mosaic of ALI data created with regression tree normalization is virtually seamless when compared with a mosaic of the clear image parts in which no normalization has been applied (Fig. 3). Regression tree normalization minimizes phenological differences between the image dates that compose cloud-cleared image mosaics (Helmer & Ruefenacht, 2007), including for LDCM-like imagery. It thereby can produce relatively seamless data.

Seamless image mosaics can be important when mapping forest attributes with limited plot data, because seams that are apparent in mosaics or composites may also appear in maps resulting from such imagery. Specialized applications that require visual interpretation to collect training data, or to delineate specific disturbances or land uses, can also benefit from relatively seamless imagery. This study is an example of such a specialized application. In the mosaics, the seams that do occur come from residual errors in the normalization models. These seams are least apparent when the image dates that form each mosaic have similar sun-target-sensor geometry (Helmer & Ruefenacht, 2007). Correcting input images for such differences

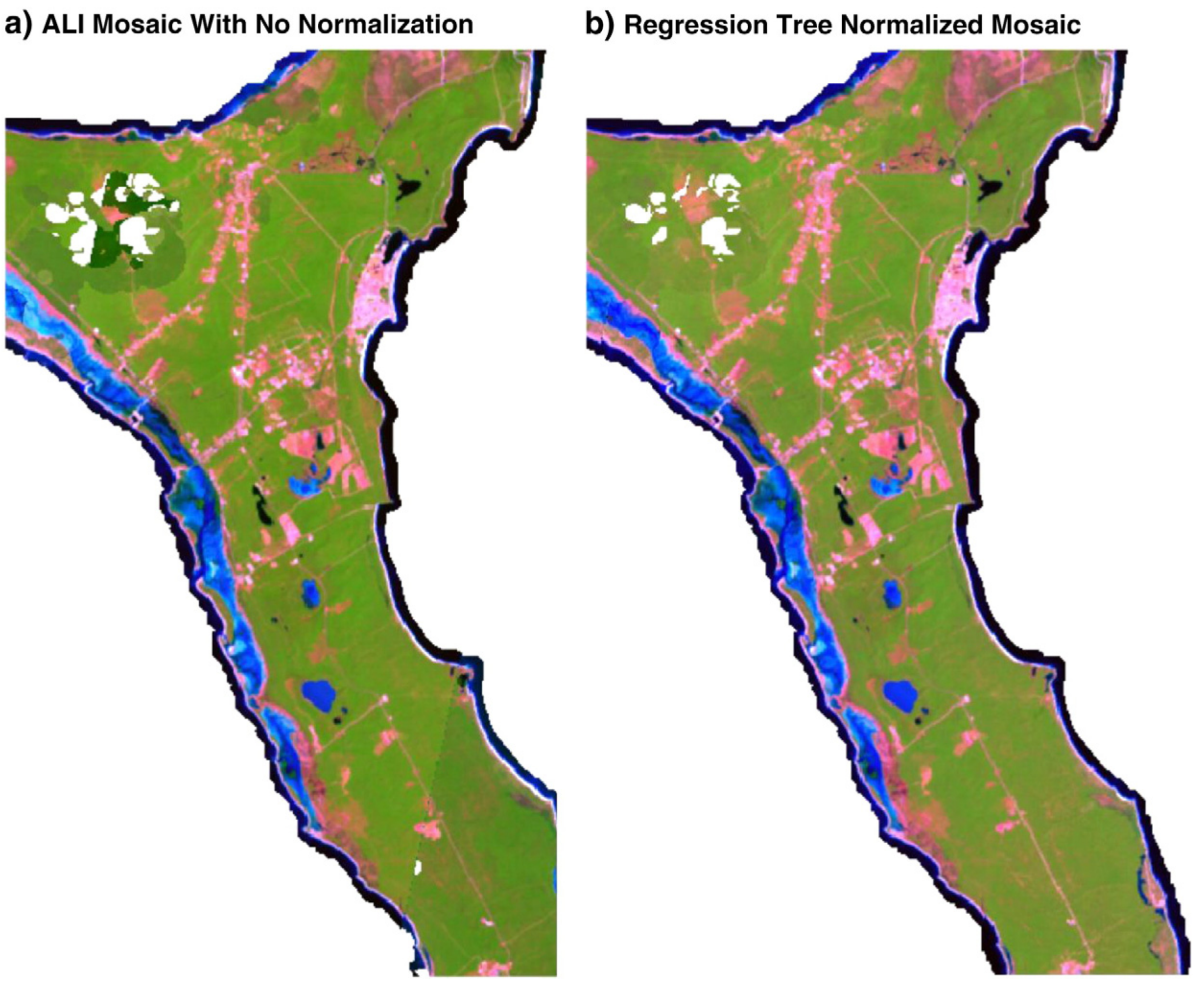

Fig. 3. A visual comparison two mosaics of the clear parts of four dates of Advance Land Imager (ALI) imagery made without (a) vs. with (b) regression tree normalization (displaying ALI bands MS5, MS4 and MS3 in RGB). The comparison suggests that cloud-cleared ALI image mosaics in tropical dry forest regions can be virtually seamless when compared with mosaics made without normalization.

would likely improve results when applying regression tree normalization. Though the method is often effective at matching nonlinear differences in vegetation phenology, results also improve when input images have similar phenology. Because the normalized data that fill cloud gaps lose some detail (Helmer & Ruefenacht, 2005), the method is only appropriate for creating mosaics from adjacent scenes if the area of interest in the adjacent scene is small. Finally, we have observed that seams occur when true land-cover change has occurred between the image dates that compose a mosaic.

3.2. Map of forest disturbance type and age

This study presents for the first time an approach for simultaneously mapping land cover and tropical forest disturbance type and age with a cloud-cleared image time series. The resulting map for Eleuthera (Fig. 4) which is based on mapping Model 1 in Table 2, is generally accurate. Overall accuracy estimated by withholding 30% of training data is 88%. Overall accuracy estimated with the stratified random sample of the classified map is 87%, and the Kappa

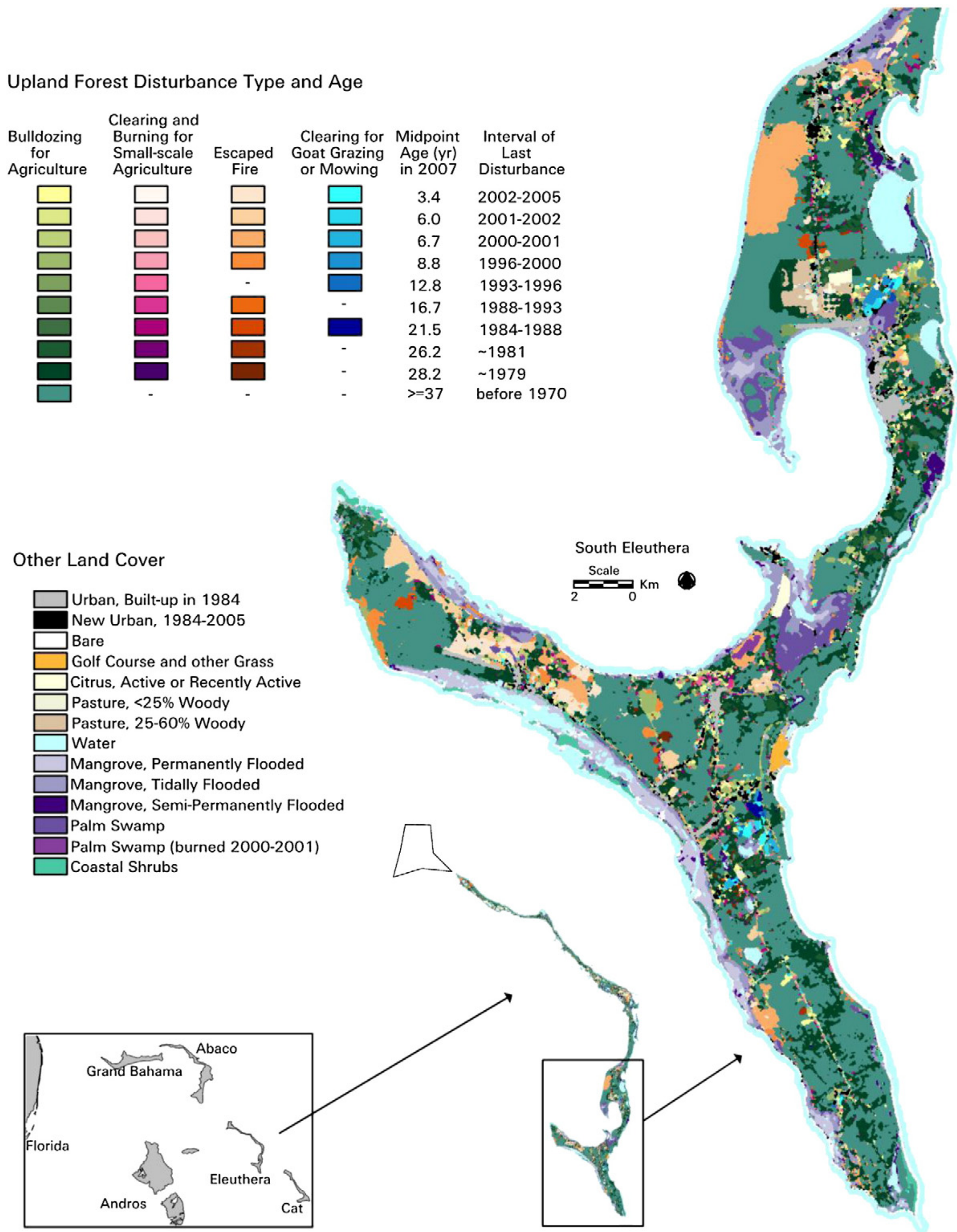

Fig. 4. Forest disturbance type and age were simultaneously mapped with supervised decision tree classification of an eight-step time series of cloud-cleared Landsat and ALI imagery. In the images, cloudy areas in a base scene for each time step are filled with clear data from other images and made seamless via the regression tree normalization method of Helmer and Ruefenacht (2005).

Table 4
Class accuracies and areas for the classes that we simultaneously mapped with decision tree classification of a time series of cloud-cleared image mosaics. These accuracies are from the stratified random sample of 1035 points, for which overall classification accuracy was 87%, and the Kappa coefficient was 0.86. The validation data combined points from land bulldozed for agriculture with points from land that did not undergo bulldozing when cleared.

Class of land cover or forest disturbance interval and type	User's accuracy (%)	Producer's accuracy (%)	Number of reference points	Class area (ha)	
				Bulldozed	Not bulldozed
Forest cleared for agriculture 2002–2005	69	50	38	431	21
Forest cleared for agriculture 2001–2002	100	87	13	118	12
Forest cleared for agriculture 2000–2001	74	88	26	373	20
Forest cleared for agriculture 1996–2000	47	84	20	815	27
Forest cleared for agriculture 1993–1996	83	95	41	245	70
Forest cleared for agriculture 1988–1993	88	100	35	293	80
Forest cleared for agriculture 1984–1988	89	81	51	154	260
Forest cleared for agric. ~1981 (active in 1984)	97	75	39	885	56
Forest cleared for agric. ~1979 (young in 1984)	65	100	20	3573	3
Forest burned 2002–2005	100	70	42	470	
Forest burned 2001–2002	97	100	29	393	
Forest burned 2000–2001	97	91	36	1310	
Forest burned 1996–2000	93	75	37	630	
Forest burned 1988–1993	90	88	30	210	
Forest burned 1984–1988	100	81	20	87	
Forest burned ~1981 (burned just before 1984)	50	19	3	21	
Forest burned ~1979 (young in 1984)	100	86	13	51	
Forest burned 2001–2002 and 2002–2005	100	100	27	68	
Forest burned 2000–2001 and 2002–2005	100	85	32	183	
Forest cleared 2002–2005 and goat grazed	83	93	21	146	
Forest cleared 2001–2002 and goat grazed	78	80	8	96	
Forest cleared 2000–2001 and goat grazed	100	80	8	71	
Forest cleared 1996–2000 and goat grazed	50	85	5	74	
Forest cleared 1993–1996 and goat grazed	75	100	3	18	
Forest cleared 1988–1993 and goat grazed	80	100	4	27	
Forest cleared ~1981 and goat grazed	90	100	9	59	
Forest undisturbed since ~1970	98	95	60	11,866	
Urban, built-up in 1984	43	79	20	1194	
New urban, 1984–2005	75	47	40	873	
Water	100	97	37	7664	
Bare	90	96	30	1788	
Golf course and other grass	96	100	22	53	
Citrus, active or semi-active				126	
Pasture, <25% woody	87	52	40	595	
Pasture, 25–60% woody	38	69	11	225	
Mangrove, Permanently flooded	57	57	30	866	
Mangrove, tidally flooded	77	87	29	1843	
Mangrove, semi-permanently flooded	67	100	20	594	
Palm swamp	97	88	31	794	
Palm swamp (burned 2000–2001)	100	60	19	41	
Coastal shrubs	93	60	36	453	

coefficient of agreement came to 0.86 (Table 4). Most classes have user's and producer's accuracy better than 70%. A patch-level evaluation of goat-grazed stands suggests good producer's accuracy. The map misclassified only two goat-grazed patches as cleared for agriculture; most age assignments of goat-grazed patches were correct. Small, scattered patches of vegetation around residential areas and some agriculture are misclassified as goat-grazed, though, suggesting commission error for the goat-grazed disturbance type. We observed that the unedited classification overestimates forest age of former citrus fields cleared well before abandonment. This observation suggests that the decision tree model mainly assigns age based on a spectral signature that is typical of a given disturbance type in a given mosaic date. It also implies that this method may inaccurately map forest age where forest age is not nearly equal to disturbance age.

We attribute the high accuracy of the map of land cover and forest disturbance type and age to six factors. First, spectral-temporal signatures from an image time series can better distinguish forest disturbance type and age than can single-date signatures. The classification based only on the image mosaic from 2002 has an overall accuracy of 44% (Model 2, Table 2), which is much worse than the overall accuracy of 83% for the classification based on the image series extending from 1984 to 2002 (Model 3, Table 2). Second, the classification is decision-tree based. Decision trees do not assume that input data are parametric, and they can accommodate nonlinear relationships between spectral data and class assignment (Friedl & Brodley, 1997). Third, the training data were comprehensive: we distributed them throughout the study area. Fourth, the seamlessness of the cloud-cleared imagery produced with regression tree normalization greatly facilitated training data collection (Helmer & Ruefenacht, 2007). Fifth, the validation points included some points that came from within the same patch, which would tend to improve accuracy estimates. Finally, visual interpretation of forest disturbance age in the reference data, and of disturbance types before about 1996, mimicked that of training data, which likely also improved accuracy estimates. All other reference classes were assigned based on field visits and interpretation of Quickbird imagery.

The disturbance map proved invaluable for characterizing Kirtland's Warbler habitat based on canopy height and disturbance type and age. By comparing warbler capture sites with the randomly selected sites, Wunderle et al. (2010) established that the warbler was linked to human-disturbed sites with low canopy height and age range of 3–28 years. Now that we have quantified some important traits of the warbler's habitat, the location and extent of potential habitat available on southern Eleuthera can be determined. More extensive vegetation data are becoming available that may permit further refinement

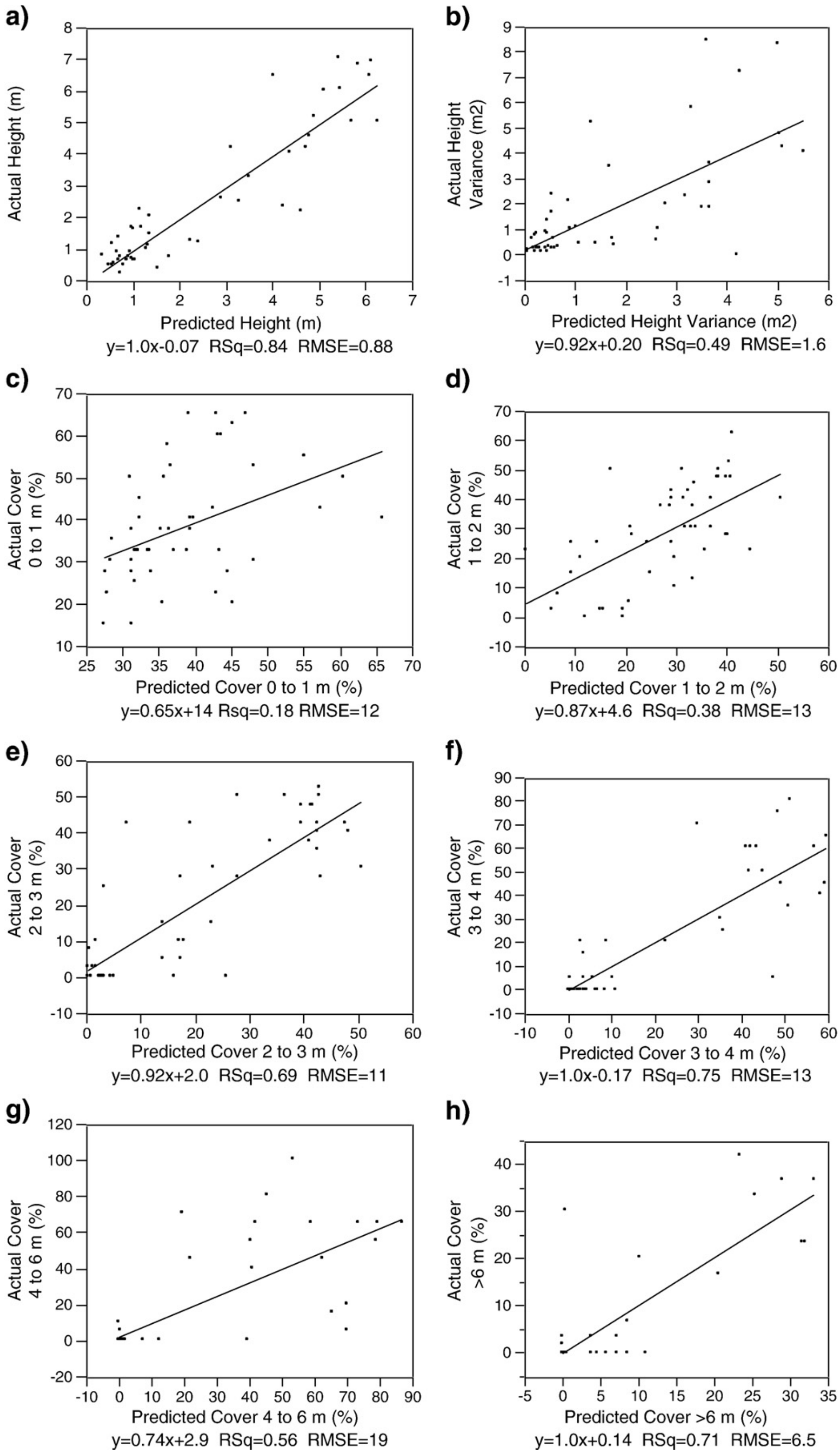

Fig. 5. Actual values for mean forest height (a), height variance (b) and percent foliage cover over vertical intervals (c through h) are plotted against values predicted by regression tree mapping models. The mapping models are based on the eight-step time series of cloud-cleared Landsat TM, ETM+ and ALI image mosaics and the field data from 48 plots. Predicted values are based on a 10-fold cross-validation.

of habitat mapping by mapping the distribution of the warbler's fruit or forage plants.

3.3. Maps of forest height and other variables from foliage height profiles

No previous studies map forest height and foliage height profiles with optical image time series. Mean height of the foliage height profiles, as predicted by the regression tree mapping model that included all mosaic dates (Model 4, Table 2), explains 84% of the variability in actual mean height, based on a 10-fold cross-validation. The root mean square error (RMSE) of the relationship is 0.9 m, and bias is negligible (Fig. 5a). In addition, the map of forest height has no discontinuities associated with the different image dates that compose the cloud-cleared imagery (Fig. 6a).

A regression tree mapping model for forest height that uses only bands from the ALI mosaic (Model 5, Table 2) predicts only 68% of the variability in actual height (10-fold cross-validation). This result indicates that the earlier imagery in the time series improves the mapping model of forest height. Supporting this conclusion is the fact that if we exclude the eight plots that were newly disturbed in the ALI mosaic and estimate a regression tree model with the cloud-cleared TM and ETM+ image mosaic from 2002 (Model 6, Table 2), the resulting model predicts only 16% of the variability in actual height (also a 10-fold cross-validation). Excluding the eight plots does not change the range of the response variable in this model and so does not explain the difference in model fits. Adding spectral data from all of the earlier TM and ETM+ image time steps (Model 7, Table 2) improves this R-square to 53%, also indicating the importance of an image time series. Given that the ALI mosaic is closer in time to when we measured

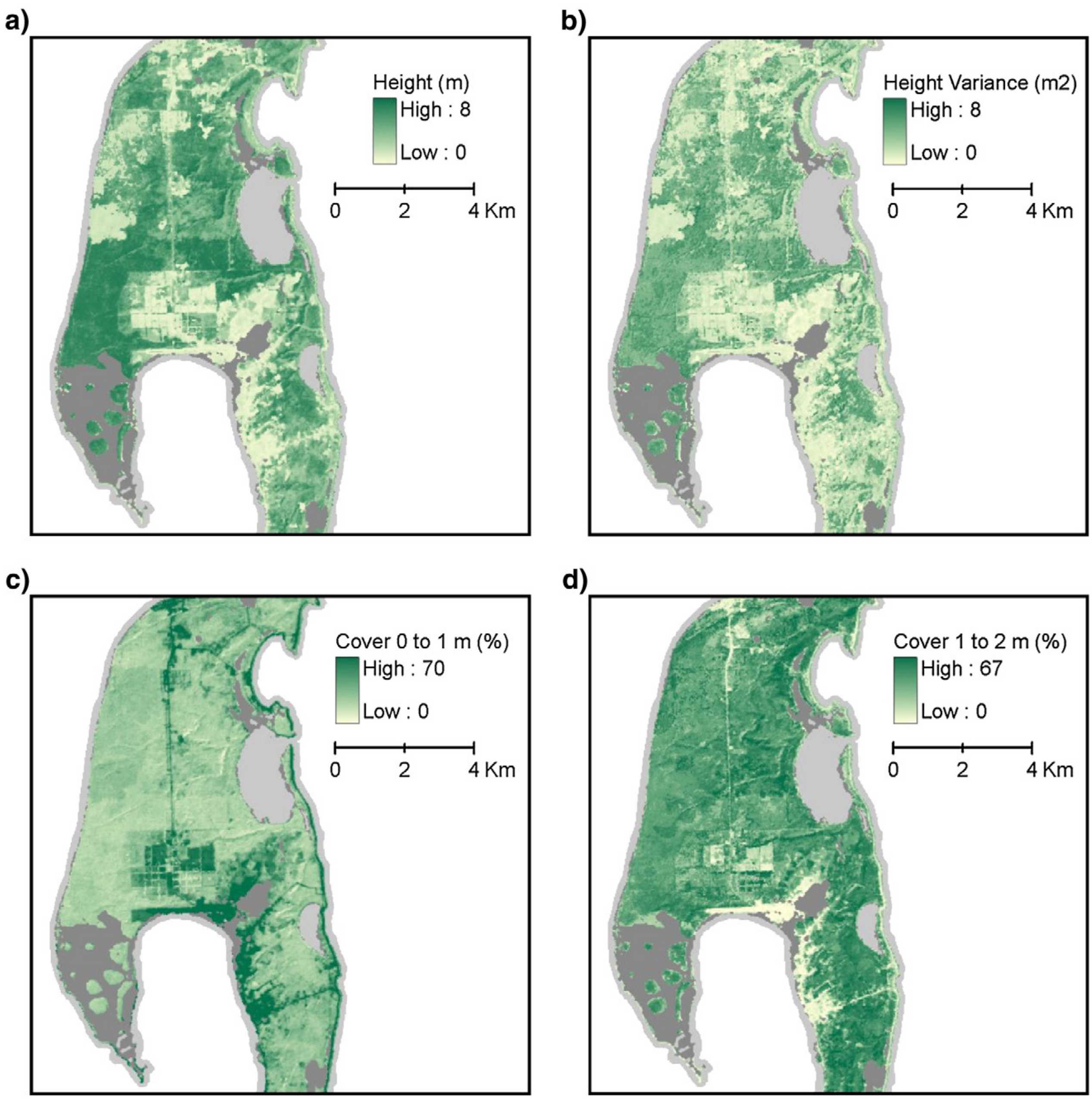

Fig. 6. Forest three-dimensional structure, including height, height variance, and percent cover over vertical intervals, was mapped from regression tree mapping models of foliage height profile data and a time series of cloud-cleared imagery, substituting time for vertical canopy space. Principal components transformation of the foliage height profile data (Fig. 7) suggest that the most variance in the data comes from contrasting foliage cover below 1 m with cover above 1 m, and this contrast is apparent in the maps (compare figure c with figures d through h).

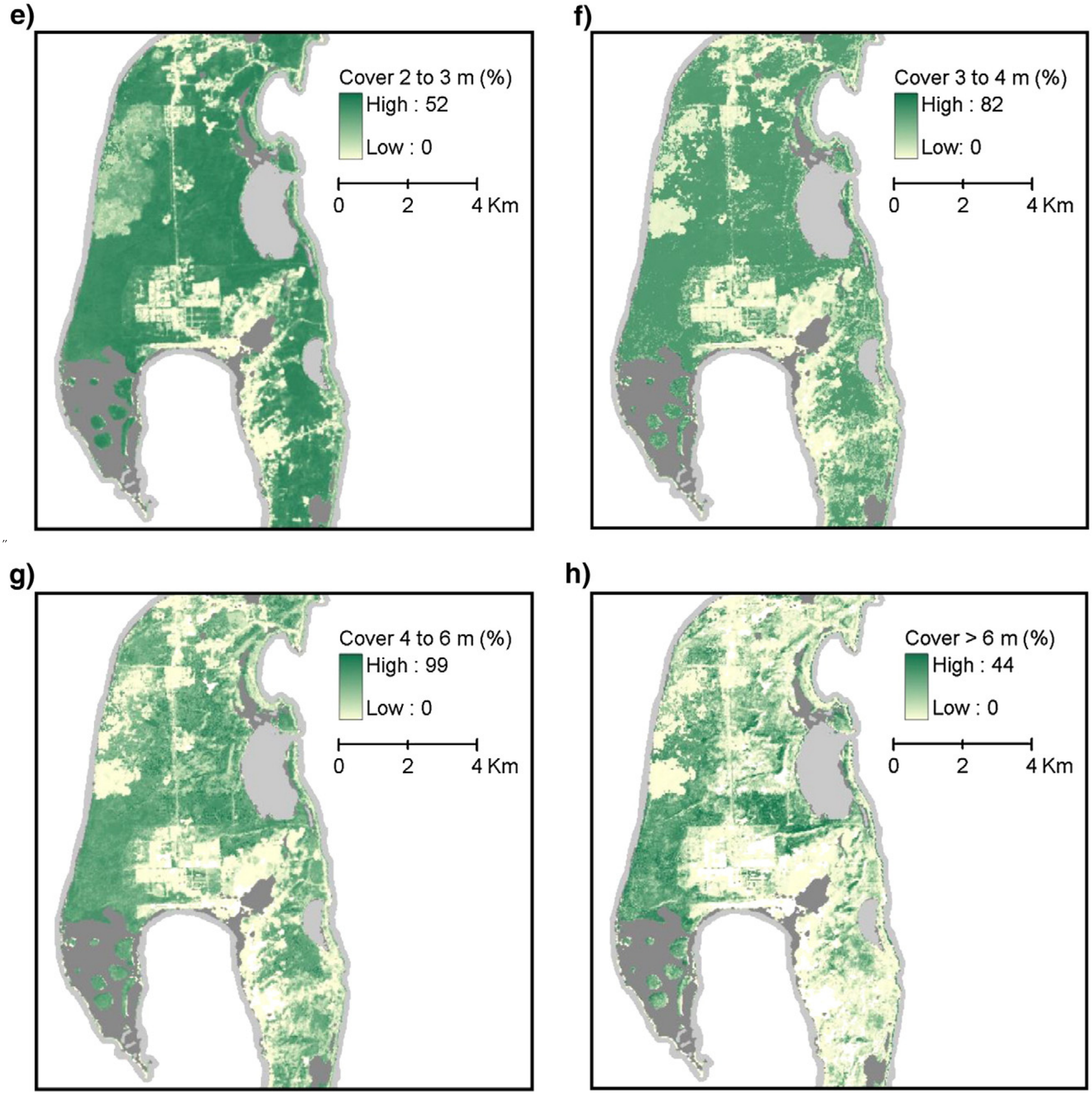

Fig. 6 (*continued*).

height, models based only on the TM and ETM+ time series are not entirely comparable to the model based only on the ALI image mosaic. However, the above results also suggest that the 12-bit ALI imagery is more sensitive to forest structure than one or more dates of TM or ETM+ imagery, which are 8-bit data. The result is consistent with results of Pu et al. (2005), who show that ALI imagery is more sensitive to forest leaf area index and crown cover than is Landsat ETM+ imagery. The NDSI calculated from ALI was the most important of the 74 spectral bands in the mapping model of forest height, occurring in rules or linear models that covered over 60% of cases. In turn, forest height was the most important predictor of height variance and canopy cover in height intervals above 2 m. The observation supports the concept that forest height explains much of the variability in forest canopy height profiles (Lefsky et al., 2005).

For percent cover over various height intervals (Fig. 5c–h), the regression tree mapping models also have negligible bias, with the exception of the mapping model for cover from 0 to 1 m. Model predictions, however, had varying precision. Model-predicted values explained 18%, 38%, 69%, 75%, 56% and 71% of the variability in actual values of percent cover from 0 to 1, 1 to 2, 2 to 3, 3 to 4, 4 to 6 and >6 m (10-fold cross-validations). Predicted height variance explained 49% of the variability in actual values. The maps of foliage height profiles were mostly seamless (Fig. 6c–h), presumably because the cloud-cleared imagery created with regression tree normalization were also nearly seamless. Only the map of percent cover from 1 to 2 m shows slight discontinuities associated with cloud-filled areas in one of the mosaics.

Like other work (Helmer et al., 2000, 2009; Helmer & Ruefenacht, 2005; Song et al., 2001), mapping from a time series of two or more images (or image mosaics) required no radiometric normalization among the time steps. That step is not necessary when the spectral values that parameterize a classification model come from the images undergoing classification rather than a different image date, a theoretical model, or a spectral trend from an image series.

3.4. Mapping forest height with image time series in other tropical landscapes

Results and observations from work here and in Amazonia suggest that three main factors help make the methods in this study effective at mapping forest vertical structure. The factors are: 1) a strong relationship between forest height and recent spectral signatures, 2) a strong relationship between forest height and past signatures, and 3) a balanced sample design. Below we discuss how these factors apply in Eleuthera and where their absence might make these methods less effective.

As for recent signatures, the first factor, the relationship between forest height and the NDSI from ALI is strong in Eleuthera; the NDSI explains 62% of the variance in a linear regression model of forest height (Table 5, Models 1, 3 and 5). The methods in this study might falter where the relationship between forest height and recent spectral data is weaker, as is likely for imagery with a smaller dynamic range than ALI has, and is possible in landscapes more humid than Eleuthera. In wetter landscapes, forests of different heights may be less spectrally distinct, as canopies close at younger ages and forests grow taller after canopy closure than the tallest forests currently in Eleuthera. In addition, active fields, woody agriculture, or pastures may have dense vegetation cover that is spectrally similar to young forest, particularly in wet season imagery.

Spectral data from past scenes (factor 2) in Eleuthera also relate well to forest height. They improve regression tree models of forest height and relate consistently to forest disturbance type and forest age, which are variables that also predict forest height (Table 5, Models 1–4). In contrast, in humid forests of Amazonia the time difference between forest clearing and agricultural abandonment varies across the landscape. Accurately mapping forest age there, for example, requires a method that finds when forest regrowth begins rather than when forests are disturbed (e.g., Helmer et al., 2009). Presumably, where forest age and disturbance age are unequal, predicting forest height will require a more precise gauge of forest age or growth than a past disturbance signature.

As to the third factor, sample design, we maximized model efficiency by stratifying the sampling of plots by two variables that we expected to explain the most variability in forest height: disturbance type and forest age. The forest height models might explain less variability in forest height with a more comprehensive sample of undisturbed forests, as would have resulted from a systematic landscape sample. Natural height differences in closed forest undergoing only subtle disturbances may not be spectrally distinct and could add unexplained variability to forest height models. Floodplain forests in Amazonia, for example, are shorter than upland forests (Helmer et al., 2009), but they are not always spectrally distinct from them.

Though disturbance type and age can predict forest height, explaining 85% of its variability, the map of forest height based on spectral data is more realistic than what would result if we mapped forest height from the thematic classes alone. For example, the forest height map from regression tree models of spectral data (Fig. 5a) maps more severely burned areas as shorter in the large area burned by escaped fire between 2000 and 2001 that is visible in the upper left part of Fig. 1f and g. A map based only on disturbance type and age would show uniform height for that entire patch. In field observations, severe burns kill more stems that would otherwise quickly resprout.

Table 5
Least squares regression models of forest mean height estimated to help explain the results of the regression tree mapping models of forest height and elucidate the relationships between forest height, age and disturbance type. The models come from the 48 field-measured foliage height profiles. All models are highly significant ($p<0.0001$), based on F-tests for overall significance of the regressions. In Models 1 and 2, forest undisturbed during the image sequence is the base case for disturbance type and represented by the intercept.

Regression models of forest height[a]	Adjusted R-square
(1) Height in m $= -3.85^{**} + 0.0026^{***}$NDSI[b] $- 0.72^{***}$Clear $-$ 0.42Fire $- 1.37^{***}$Goat	0.87
(2) Height in m $= 1.12^{***} + 0.10^{***}$Age $- 0.47^{*}$Clear $+$ 0.37Fire $- 1.29^{***}$Goat	0.85
(3) Height in m $= -3.57^{*} + 0.17^{**}$NDSI[b] $+ 0.12$Age***	0.81
(4) Height in m $= 0.11 + 0.15^{***}$Age	0.79[c]
(5) Height in m $= -10.06^{***} + 0.0049^{***}$NDSI[b]	0.62[c]

[a] Asterisks indicate probabilities of erroneously rejecting the null hypothesis that coefficient estimates are zero, based on a two-sided *t*-distribution, $^{***}p\le0.0005$, $^{**}p\le0.005$, $^{*}p\le0.05$.
[b] NDSI = normalized difference structure index in ALI imagery, rescaled to 12 bits.
[c] R-square shown rather than Adjusted R-square.

3.5. Relationships between forest vertical structure and Kirtland's Warbler forage species

The PCA of the foliage height profiles, with disturbance type identified, shows the landscape–level relationships between forest vertical structure, disturbance type and counts of Kirtland's Warbler forage species and *L. leucocephala*. The axis shows a gradient that is important to Kirtland's Warbler habitat. The first component (PC1) explains 43% of the total data variability. It separates stands with dense foliage cover in the height interval from 0 to 1 m from taller stands with less cover near the ground (Fig. 7a). The PC1 axis also shows that *L. bahamensis*, *L. leucocephala* and *L. involucrata* are associated with these short stands, while *C. alba* is associated with stands that have dense foliage cover from 1 to 4 m. The shortest stands include young stands cleared for agriculture, young stands burned from escaped fire, and both young and old goat-grazed stands (Fig. 7b).

The second PC axis (PC2) explains 17% more variation in the data. It also shows an important habitat gradient. The PC2 axis separates stands with high counts of *L. involucrata* from stands with more *L. bahamensis* and *L. leucocephala*. One of the most important fruit species for the Kirtland's Warbler is *L. involucrata* (Wunderle et al., 2010). A hypothesis is that *L. involucrata* is more common in those goat-grazed patches subject to ongoing goat grazing (or patches subject to periodic mowing, based on the presence of *L. involucrata* along mowed roadsides), but less abundant where goats have recently been excluded. Goats browse and disperse *L. leucocephala*; being a legume, its nutrient content is relatively high (Clavero & Razz, 2003; Pamo et al., 2006). Consequently, we expect it to be less abundant in patches subject to more intense or ongoing goat grazing, allowing *L. involucrata* to thrive.

3.6. Forest disturbance rates in South and Central Eleuthera

Forest disturbance rates changed in South and Central Eleuthera from 1984 to 2005 (Fig. 8). Disturbance rates tended to be largest for agriculture associated with bulldozing (Agriculture 1) before about the year 2000, averaging 107 ha year^{-1} over the four intervals before the year 2000. Forest disturbance for agriculture with bulldozing increased to an average of 207 ha year^{-1} over the three intervals since 2000. However, escaped fire became the largest source of forest disturbance after 2000, increasing 9-fold from an average of 65 ha year^{-1} before then to an average of 579 ha year^{-1} after. Four hurricanes brushed or hit Eleuthera from 1999 to 2004. Hurricane Floyd hit Eleuthera in September 1999 with sustained winds of 120 miles per hour and is considered the most destructive hurricane to hit the region since 1929, suggesting that the increase in area disturbed by escaped fire might stem mainly from increased fuel loadings caused by hurricane disturbance, though the concurrent increase in forest clearing for agriculture is probably also important. Forest clearing for goat grazing increased somewhat after around the year 2001.

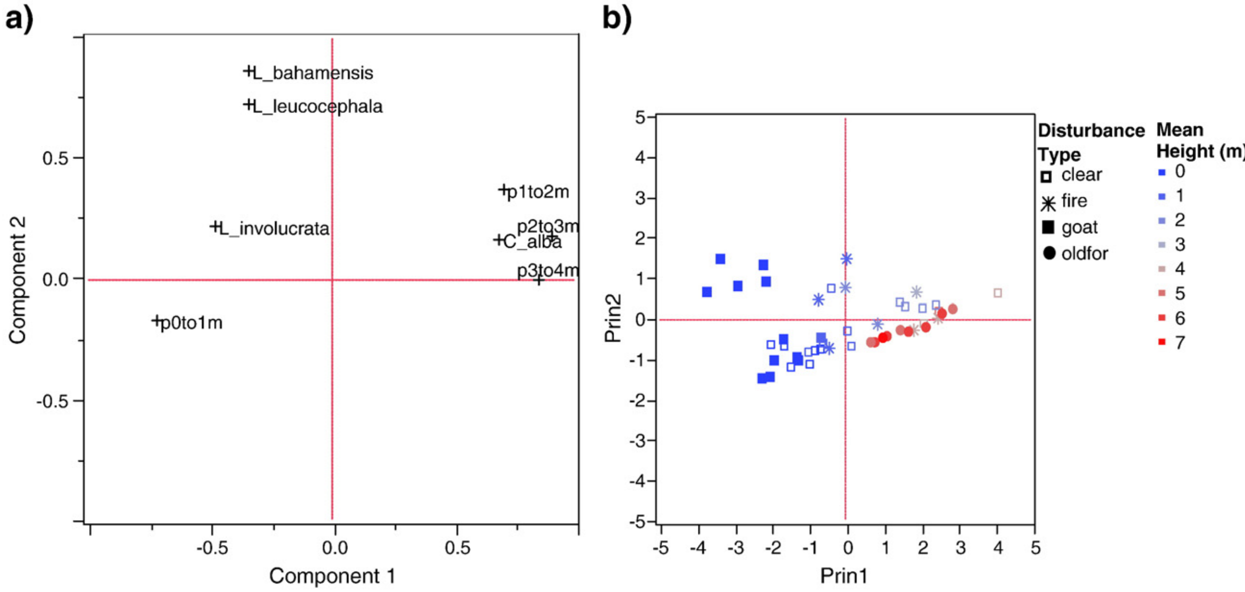

Fig. 7. A principal components analysis of foliage height profile data illustrates the relationships between forest vertical structure, disturbance type, and counts of woody species that provide important Kirtland's Warbler forage as well as a potentially competing species. Disturbance types include clearing for agriculture (clear), burning by escaped fire (fire), clearing followed by regrowth with goat grazing (goat) and forest undisturbed during the image sequence (oldfor).

4. Summary and conclusions

This study shows that time, as gauged by a multiyear time series of cloud-cleared satellite imagery, can be exchanged for continuous vertical forest canopy space. We map aspects of forest three-dimensional structure: mean height ranging from 0.6 to 7 m; height variance; and percent cover in vertical intervals. We conclude that forest height mapping is possible with a time series of ALI and TM or ETM+ imagery in subtropical dry forest landscapes on limestone substrate where forest height relates strongly to recent and past spectral data. Both an image time series and ALI data may be critical to accurately mapping forest height. Models based only on one image time step or that exclude the ALI data are much weaker. The OLI imagery from the next Landsat mission will likely improve our ability to map forest vertical structure. However, our results also highlight that a Landsat archive that includes many past images will maximize the utility of the forthcoming OLI data for monitoring forest structure.

This study also demonstrates the usefulness of long, dense time series of cloud-cleared Landsat and ALI images made with regression tree normalization. Seven of the eight steps in the image time series with which we map forest vertical structure are cloud-cleared image mosaics. Although only 48 forest plots were available to calibrate the mapping models for height and other variables, the resulting maps have few discontinuities associated with the different dates that compose the mosaics in the time series. This observation supports regression tree normalization as an option for producing cloud-cleared image mosaics for mapping forest attributes with models based on limited field data. Unlike methods that rely on MODIS to

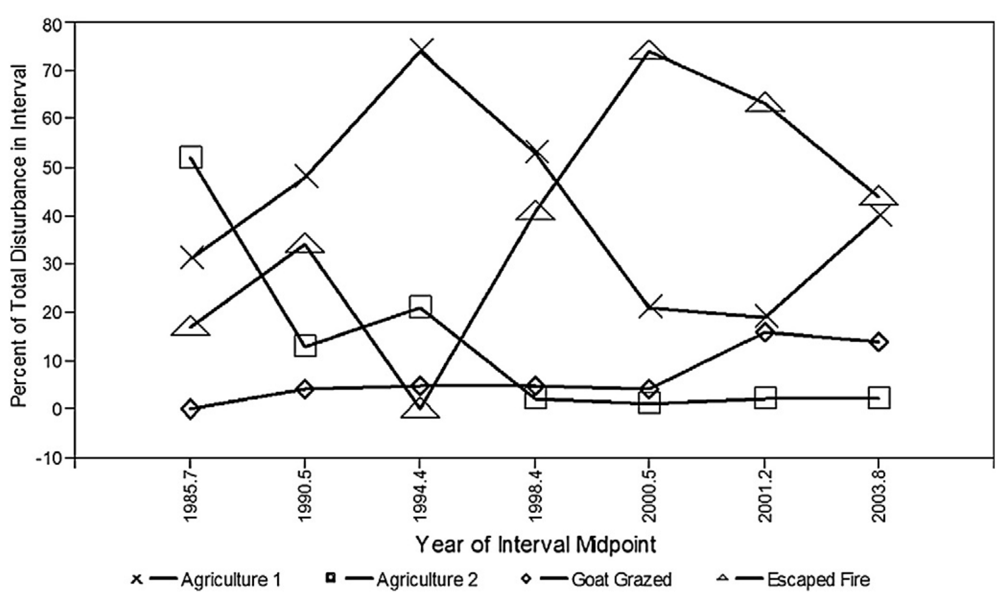

Fig. 8. Forest disturbance rates are shown here as the percent of the total area of forest disturbed during each interval. The percentages are calculated from the data in Table 6. Disturbance patterns changed in South and Central Eleuthera from 1984 to 2005. Before the year 2000, disturbance rates in ha year^{-1} tended to be largest for agriculture associated with bulldozing (Agriculture 1). After about the year 2000, forest disturbance by escaped fire averaged 579 ha year^{-1} and was the largest source of forest disturbance. Forest clearing for goat grazing increased somewhat around 2001.

Table 6
Disturbance rates for Central and South Eleuthera Island, The Bahamas, 1984–2005, calculated as the number of ha disturbed during an interval (from Table 3) divided by the interval length. Agriculture 1 includes clearing that involved bulldozing, whether for agriculture or for urban development that did not ensue, and including citrus plantations (for which we manually determined the date of initial forest clearing). Agriculture 2 includes small-scale agriculture that did not obviously undergo bulldozing. Clearing for goat grazing includes cleared forest that regrew under pressure of goat grazing. Escaped Fire includes lands burned by fire that escaped from agricultural burning.

Interval years	Interval length (yr)	Clearing for Agriculture 1, bulldozed (ha year^{-1})	Clearing for Agriculture 2, not bulldozed (ha year^{-1})	Clearing for goat grazing (ha year^{-1})	Burned by Escaped Fire (ha year^{-1})	Total area of forest disturbed during interval[a] (ha)
1984–1988	4.5	34	58	0	19	111
1988–1993	4.9	60	16	6	43	124
1993–1996	3.1	79	23	6	0	107
1996–2000	3.2	255	8	23	197	483
2000–2001	1.0	373	20	71	1310	1774
2001–2002	1.7	69	7	56	231	364
2002–2005	2.4	180	9	61	196	445

[a] Excludes land converted to urban/built-up land, most of which was forest, which occurred at an average rate of 873 ha/20.8 years, or 42 ha year^{-1}.

normalize the data that fill cloud gaps, the regression tree method is applicable to imagery dated before the year 2000. The ability of the regression tree method to provide cloud-cleared data dated from before the year 2000 was critical to the study.

Our results also show that digital classification of a time series of cloud-cleared Landsat and ALI images can simultaneously map land cover and forest disturbance type and age. The image time series and comprehensive training data were important to this result. Collecting the training data required visually identifying forest disturbance events, disturbance types, and regrowth. Enhancing this visualization were the relatively seamless cloud-cleared image mosaics and viewing the imagery as a series of RGB wetness composites. The results of this study also suggest that the regression tree-normalization method of Helmer and Ruefenacht (2005) will be effective with the forthcoming 12-bit OLI data that the LDCM mission will provide. The regression tree normalization method is completely automatic. However, operationally producing mosaics based on the method requires accurate cloud and cloud shadow masks, which we did not produce automatically in this study.

The map of forest disturbance type and age includes specialized disturbance classes, like forest clearing followed by goat grazing, which fully automated algorithms for forest change detection are unlikely to distinguish from other disturbance types. This specialized disturbance type of clearing followed by goat grazing is associated with important Kirtland's Warbler forage species, including *L. involucrata* and, according to earlier work, *E. fruticosa* (Wunderle et al., 2010). The goat grazing and browsing apparently stunt these forests, because even older stands remain short, and may reduce competition from nonforage species.

Given that visual interpretation was important to mapping forest disturbance type and age, we also conclude that a global archive of Landsat image time series should include relatively seamless cloud-cleared imagery for time intervals with no completely clear scenes but several partly cloudy ones. Producing such imagery will require accurate automated cloud and cloud shadow detection. Fully automated algorithms exist that do not require mosaics to map general aspects of forest disturbance from image time series. However, no single algorithm will satisfy the myriad of specialized applications that are possible with time series of satellite imagery. With readily available image time series that include seamless cloud-cleared imagery for persistently cloudy regions, users can more easily tailor classifications to specialized needs.

Acknowledgements

This research is a contribution to the Landsat Data Continuity Mission (LDCM) and Landsat Science Team Research. We conducted it in cooperation with the USFS Rocky Mountain Research Station (RMRS), the University of Puerto Rico, The College of The Bahamas, The Bahamas National Trust, and the Kirtland's Warbler Recovery Team. From RMRS we thank David Turner, Laurie Porth, Rudy King, L. Scott Baggett, Ray Czaplewski and Kathleen Dwire for input on sample design and analyses. Thanks also to Michael Lefsky for input on measurement and analysis of foliage height profiles, to Javier Mercado for assistance with data entry and summarization, and to Ty Wilson and Rachel Riemann for input on mapping models. From CEMML of CSU, thanks to Calvin Bagley and Gary Senseman, and to Marie Held for assistance with figures. Rudy Bahia, Samara Lawrentz, Montara Roberts, and Jennifer White assisted with field measurements. Justin D. Gray also assisted with fieldwork and provided volunteer IT support. International Programs of the USDA Forest Service provided partial funding through the Puerto Rican Conservation Foundation. The USGS and the Landsat Science Team provided the Landsat and ALI data. Four anonymous reviewers improved the manuscript. Colors for the land-cover map were inspired by or came from Colorbrewer2 (http://colorbrewer2.org).

References

Bergen, K. M., Gilboy, A. M., & Brown, D. G. (2007). Multi-dimensional vegetation structure in modeling avian habitat. *Ecological Informatics*, *2*, 9—22.

Chopping, M., Nolin, A., Moisen, G. G., Martonchik, J. V., & Bull, M. (2009). Forest canopy height from the Multiangle Imaging SpectroRadiometer (MISR) assessed with high resolution discrete return lidar. *Remote Sensing of Environment*, *113*, 2172—2185.

Clavero, T., & Razz, R. (2003). The performance of goats browsing *Leucaena leucocephala* in the semi arid areas of northwest Venezuela. *Revista Científica*, *13*, 460—463.

Cohen, J. (1960). A coefficient of agreement for nominal scales. *Educational and Psychological Measurement*, *20*, 37—46.

Crist, E. P., & Cicone, R. C. (1984). A physically-based transformation of Thematic Mapper data—The TM tasseled cap. *IEEE Transactions on Geoscience and Remote Sensing*, *22*, 256—263.

Crist, E. P., Laurin, R., & Cicone, R. C. (1986). Vegetation and soils information contained in transformed Thematic Mapper data. *Geoscience and Remote Sensing Symposium, 1986. IGARSS '86* (pp. 1465—1470). Paris, France: ESA.

Czaplewski, R. L. (2003). Accuracy assessment of maps of forest condition, statistical design and methodological considerations. In M. A. Wulder, & S. E. Franklin (Eds.), *Remote sensing of forest environments: Concepts and case studies* (pp. 115—140). Norwell, MA: Kluwer Academic Publishers.

ERDAS, I. (2008). *Imagine Autosync guide.* Norcross, GA: ERDAS, Inc.

Fiorella, M., & Ripple, W. J. (1993). Analysis of conifer forest regeneration using Landsat thematic mapper data. *Photogrammetric Engineering and Remote Sensing*, *59*, 1383—1388.

Fiorella, M., & Ripple, W. J. (1993). Determining successional stage of temperate coniferous forests with Landsat satellite data. *Photogrammetric Engineering and Remote Sensing*, *59*, 239—246.

Friedl, M. A., & Brodley, C. E. (1997). Decision tree classification of land cover from remotely sensed data. *Remote Sensing of Environment*, *61*, 399—409.

Gao, F., Masek, J. G., Schwaller, M., & Hall, F. (2006). On the blending of the Landsat and MODIS surface reflectance: predicting daily Landsat. *IEEE Transactions on Geoscience and Remote Sensing*, *44*, 2207—2208.

Goetz, S., Steinberg, D., Dubayah, R., & Blair, B. (2007). Laser remote sensing of canopy habitat heterogeneity as a predictor of bird species richness in an eastern temperate forest, USA. *Remote Sensing of Environment*, *108*, 254—263.

Gottschalk, T. K., Huettmann, F., & Ehlers, M. (2005). Review article: Thirty years of analysing and modelling avian habitat relationships using satellite imagery data: A review. *International Journal of Remote Sensing*, *26*, 2631—2656.

Hansen, M. C., Roy, D. P., Lindquist, E., Adusei, B., Justice, C. O., & Altstatt, A. (2008). A method for integrating MODIS and Landsat data for systematic monitoring of forest cover and change in the Congo Basin. *Remote Sensing of Environment*, *112*, 2495—2513.

Hardisky, M. A., Smart, R. M., & Vytautas, K. (1983). Growth response and spectral characteristics of a short *Spartina alterniflora* salt marsh irrigated with freshwater and sewage effluent. *Remote Sensing of Environment*, *13*, 57−67.
Helmer, E. H. (2000). The landscape ecology of secondary forest in montane Costa Rica. *Ecosystems*, *3*, 98−114.
Helmer, E. H., Cohen, W. B., & Brown, S. (2000). Mapping montane tropical forest successional stage and land use with multi-date Landsat imagery. *International Journal of Remote Sensing*, *21*, 2163−2183.
Helmer, E. H., Brandeis, T., Lugo, A. E., & Kennaway, T. (2008a). Spatial controls on tropical forest age and implications for carbon storage and species diversity of the forests cleared for land development. *Journal of Geophysical Research. G. Biogeosciences*, *113*, G02S04.
Helmer, E. H., Kennaway, T. A., Pedreros, D. H., Clark, M. L., Marcano-Vega, H., Tieszen, L. L., et al. (2008b). Land cover and forest formation distributions for St. Kitts, Nevis, St. Eustatius, Grenada and Barbados from decision tree classification of cloud-cleared satellite imagery. *Caribbean Journal of Science*, *44*, 175−198.
Helmer, E. H., Lefsky, M. A., & Roberts, D. A. (2009). Biomass accumulation rates of Amazonian secondary forest and biomass of old-growth forests from Landsat time series and the Geoscience Laser Altimeter System. *Journal of Applied Remote Sensing*, *3*(033505), 1−31.
Helmer, E. H., & Ruefenacht, B. (2005). Cloud-free satellite image mosaics with regression trees and histogram matching. *Photogrammetric Engineering and Remote Sensing*, *71*, 1079−1089.
Helmer, E. H., & Ruefenacht, B. (2007). A comparison of radiometric normalization methods when filling cloud gaps in Landsat imagery. *Canadian Journal of Remote Sensing/Journal Canadien de Teledetection*, *33*, 325−340.
Holmes, R. T., Bonney, R. E. J., & Pacala, W. (1979). Build structure of the Hubbard Brook bird community: A multivariate approach. *Ecology*, *60*.
Huang, C., Goward, S. N., Masek, J. G., Thomas, N., Zhu, Z., & Vogelmann, J. E. (2009). An automated approach for reconstructing recent forest disturbance history using dense Landsat time series stacks. *Remote Sensing of Environment*, *114*, 183−198.
Huang, C., Wylie, B., Homer, C., Yang, L., & Zylstra, G. (2002). Derivation of a tasseled cap transformation based on Landsat 7 at-satellite reflectance. *International Journal of Remote Sensing*, *23*, 1741−1748.
Jin, S., & Sader, S. A. (2005). Comparison of time series tasseled cap wetness and the normalized difference moisture index in detecting forest disturbances. *Remote Sensing of Environment*, *94*, 364−372.
Johnston, D. W., & Odum, E. P. (1956). Breeding bird populations in relation to plant succession on the piedmont of Georgia. *Ecology*, *37*, 50−62.
Kalacska, M., Sanchez-Azofeifa, G. A., Rivard, B., Caelli, T., White, H. P., & Calvo-Alvarado, J. C. (2007). Ecological fingerprinting of ecosystem succession: Estimating secondary tropical dry forest structure and diversity using imaging spectroscopy. *Remote Sensing of Environment*, *108*, 82−96.
Karr, J. R. (1968). Habitat and avian diversity on strip-mined land in east-central Illinois. *The Condor*, *70*.
Kellndorfer, J., Walker, W., Pierce, L., Dobson, C., Fites, J. A., Hunsaker, C., et al. (2004). Vegetation height estimation from Shuttle Radar Topography Mission and National Elevation Datasets. *Remote Sensing of Environment*, *93*, 339−358.
Kennaway, T., & Helmer, E. H. (2007). The forest types and ages cleared for land development in Puerto Rico. *GIScience and Remote Sensing*, *44*, 356−382.
Kennaway, T. A., Helmer, E. H., Lefsky, M. A., Brandeis, T. A., & Sherrill, K. R. (2008). Mapping land cover and estimating forest structure using satellite imagery and coarse resolution lidar in the Virgin Islands.*Journal of Applied Remote Sensing*, *2* (023551) 1-27.
Kennedy, R. E., Cohen, W. B., & Schroeder, T. A. (2007). Trajectory-based change detection for automated characterization of forest disturbance dynamics. *Remote Sensing of Environment*, *110*, 370−386.
Kullback, S. (1959). *Information theory and statistics.* New York: John Wiley and Sons.
Leck, C. F. (1979). Avian extinctions in an isolated tropical wet-forest preserve, Ecuador. *The Auk*, *96*, 343−352.
Lefsky, M. A., Cohen, W. B., Parker, G. G., & Harding, D. J. (2002). Lidar remote sensing for ecosystem studies. *Bioscience*, *52*, 19−30.
Lefsky, M. A., Hudak, A. T., Cohen, W. B., & Acker, S. A. (2005). Patterns of covariance between forest stand and canopy structure in the Pacific Northwest. *Remote Sensing of Environment*, *95*, 517−531.
Legendre, P., & Legendre, L. (1998). *Numerical ecology.* Amsterdam: Elsevier.
MacArthur, R. H. (1958). Population ecology of some warblers of Northeastern Coniferous Forests. *Ecology*, *39*, 599−619.
Masek, J. G., Huang, C., Wolfe, R., Cohen, W., Hall, F., Kutler, J., et al. (2008). North American forest disturbance mapped from a decadal Landsat record. *Remote Sensing of Environment*, *112*, 2914−2926.
Pamo, E. T., Tedonken, F., Kana, J. R., Boukila, B., & Nanda, A. S. (2006). Effects of *Calliandra calothyrsus* and *Leucaena leucocephala* supplementary feeding on goat production in Cameroon. *Small Ruminant Research*, *65*, 31−37.
Papathanassiou, K. P., & Cloude, S. K. (2001). Single-baseline polarimetric SAR interometry. *IEEE Transactions on Geoscience and Remote Sensing*, *39*, 2352−2363.
Pu, R., Yu, Q., Gong, P., & Biging, G. S. (2005). EO-1 Hyperion, ALI and Landsat 7 ETM+ data comparison for estimating forest crown closure and leaf area index. *International Journal of Remote Sensing*, *26*, 457−474.
Rappole, J. H., & Morton, E. S. (1985). Effects of habitat alteration on a tropical avian forest community. *Ornithological Monographs*, 1013−1021.
Roy, D. P., Ju, J., Lewis, P., Schaaf, C., Gao, F., Hansen, M., et al. (2008). Multi-temporal MODIS-Landsat data fusion for relative radiometric normalization, gap filling, and prediction of Landsat data. *Remote Sensing of Environment*, *112*, 3112−3130.
Ruefenacht, B., Finco, M. V., Nelson, M. D., Czaplewski, R., Helmer, E. H., Blackard, J. A., et al. (2008). Conterminuous US and Alaska forest type mapping using forest inventory and analysis data. *Photogrammetric Engineering and Remote Sensing*, *74*, 1379−1388.
Sader, S. A., & Winne, J. C. (1992). RGB–NDVI colour composites for visualizing forest change dynamics. *International Journal of Remote Sensing*, *13*, 3055−3067.
Schemske, D. W., & Browkaw, N. (1981). Treefalls and the distribution of understory birds in a tropical forest. *Ecology*, *62*, 938−945.
Song, C., Woodcock, C. E., Seto, K. C., Lenney, M. P., & Macomber, S. A. (2001). Classification and change detection using Landsat TM data: When and how to correct atmospheric effects? *Remote Sensing of Environment*, *75*, 230−244.
Terborgh, J. (1977). Bird species diversity on an Andean elevational gradient. *Ecology*, *58*, 1007−1019.
Thiollay, J. M. (1999). Responses of an avian community to rain forest degradation. *Biodiversity and Conservation*, *8*, 513−534.
Véga, C., & St-Onge, B. (2008). Height growth reconstruction of a boreal forest canopy over a period of 58 years using a combination of photogrammetric and lidar models. *Remote Sensing of Environment*, *112*, 1784−1794.
Wilson, E. H., & Sader, S. A. (2002). Detection of forest harvest type using multiple dates of Landsat TM imagery. *Remote Sensing of Environment*, *80*, 385−396.
Wolter, P. T., Townsend, P. A., & Sturtevant, B. R. (2009). Estimation of forest structural parameters using 5 and 10 meter SPOT-5 satellite data. *Remote Sensing of Environment*, *113*, 2019−2036.
Wunderle, J., Currie, D., & Ewert, D. N. (2007). The potential role of hurricanes in the creation and maintenance of Kirtland's Warbler habitat in the Bahamas archipelago. *Proceedings of the 11th Symposium on the Natural History of the Bahamas* (pp. 121−129). San Salvador, Bahamas: Gerace Research Center.
Wunderle, J. M. J., Currie, D., Helmer, E. H., Ewert, D. N., White, J. D., Ruzycki, T. S., et al. (2010). Kirtand's warblers in anthropogenically disturbed early successional habitats on Eleuthera, The Bahamas. *The Condor*, *112*, 123−137.
Wunderle, J. M., Jr., & Waide, R. B. (1993). Distribution of overwintering Nearctic migrants in the Bahamas and Greater Antilles. *The Condor*, *95*, 904−933.
Zhang, C., Li, W., & Travis, D. J. (2009). Restoration of clouded pixels in multispectral remotely sensed imagery with cokriging. *International Journal of Remote Sensing*, *30*, 2173−2195.